Catalytic Ozonation of Selected Pharmaceuticals over Mesoporous Alumina-Supported Manganese Oxide

LI YANG, CHUN HU,* YULUN NIE, AND JIUHUI QU

State Key Laboratory of Environmental Aquatic Chemistry, Research Center for Eco-Environmental Sciences, Chinese Academy of Sciences, Beijing 100085, China

Received November 17, 2008. Revised manuscript received February 9, 2009. Accepted February 10, 2009.

Catalytic ozonation of five pharmaceutical compounds (PhACs)—phenazone, ibuprofen, diphenhydramine, phenytoin, and diclofenac sodium in alumina-supported manganese oxide (MnO_x) suspension was carried out with a semicontinuous laboratory reactor. MnO_x supported by mesoporous alumina (MnO_x/MA) was highly effective in mineralizing the PhACs in aqueous solution. Fourier transform infrared (FTIR) spectroscopy and in situ attenuated total reflection FTIR (ATR-FTIR) spectroscopy were used to examine the interaction of ozone with different catalysts under various conditions. The crucial active sites, surface oxide species at 1380 cm^{-1}, were formed by the interaction of ozone with Lewis acid sites on the alumina surface. New surface hydroxyl groups at 2915 and 2845 cm^{-1} were produced by the interaction of the catalyst and ozone in aqueous suspension and became active sites in the presence of MnO_x. The introduction of MnO_x enhanced the formation and activation of surface hydroxyl groups, causing higher catalytic reactivity. On the basis of these findings, a reaction mechanism is proposed for the catalytic ozonation of PhACs in MnO_x/MA suspension.

Introduction

Pollution from pharmaceutical compounds (PhACs) in surface and ground waters is an environmental concern in many countries (*1*−*3*). Some PhACs resist even advanced water treatment systems such as adsorption on granular activated carbon or ozonation (*4*). Only a few pharmaceuticals have been detected in drinking water to date (*5, 6*). Although concentrations of the PhACs are typically in the lower nanogram per liter range, potential dangers to humans and ecological health may exist due to long-term exposure (*7, 8*).

Heterogeneous catalytic ozonation has received increasing attention in recent years due to its potentially higher effectiveness in the degradation and mineralization of refractory organic pollutants and its lower negative effect on water quality. It was developed to overcome the limitations of ozonation processes, such as the formation of byproduct and selective reactions of ozone (*9, 10*). Supported and unsupported metals and metal oxides are the most commonly tested catalysts for the ozonation of organic compounds in water or air (*11, 12*). In many cases, alumina-supported metal oxides of iron, silver, cobalt, nickel, manganese, and copper show high activity for the destruction of pollutants with ozone at ambient temperature (*13*−*15*). Experimental results indicate that the removal efficiencies of pollutants are significantly enhanced in the presence of catalysts compared to ozone alone. The activity of the catalysts mentioned is based mainly on catalytic ozone decomposition and the enhanced generation of hydroxyl radicals. However, these results obtained from various studies suggest different ozonation mechanisms. The decomposition mechanism of gaseous ozone has been elucidated with in situ Raman spectroscopy and isotopic substitution (*16, 17*). The main redox steps were involved in the formation of superoxide or peroxide species on the surfaces of metal oxides. Bulanin et al. (*18*) suggested that ozone dissociates after adsorption on strong Lewis sites, yielding a surface oxygen atom, whereas on weaker sites, ozone molecules coordinate via one of the terminal oxygen atoms. With regard to the bulk aqueous phase, the catalytic ozonation mechanism is still controversial because the pathway is so complex, but in the heterogeneous catalytic ozonation process, adsorption of ozone and its further decomposition are generally believed to lead to surface-bound O radicals and hydroxyl radicals on the surfaces of catalysts (*19*−*21*). The surface hydroxyl groups, Brönsted and Lewis acid sites, are thought to be the centers of metal oxide (*19*). Ma and Graham reported that ozone decomposition was initiated by hydroxide ions linked to the negatively charged surface of metal oxide and that the surface hydroxyl groups formed in situ were active sites for catalytic ozonation (*20*). When introduced into water, metal oxides tend to strongly adsorb H_2O molecules. The adsorbed H_2O dissociates into OH^- and H^+, forming surface hydroxyl groups with the surface metal and oxygen sites, respectively (*22*). Therefore, the amount and the properties of the hydroxyls formed depend on the metal oxide.

The objective of this study was to study aqueous-phase catalytic ozonation of PhACs over various alumina-supported MnO_x and the catalytic ozonation mechanism at the solid−liquid interface. In the present study, synthetic mesoporous γ-Al_2O_3 (MA), commercial mesoporous γ-Al_2O_3 (CMA), and nonporous α-Al_2O_3 (CA) were examined as supports for preparing variously supported MnO_x for the catalytic ozonation of PhACs in water. Five PhACs occurring in the aquatic environment due to their widespread use in the United States and Europe (*1, 23*) were selected to help evaluate the activity and properties of the catalysts. During the degradation of PhACs with catalytic ozonation, surface changes of various catalysts were investigated using Fourier transform infrared (FTIR) spectroscopy and in situ attenuated total reflection FTIR (ATR-FTIR) spectroscopy. The latter is ideally suited for studying molecular vibrations at the solid−liquid interface because the evanescent wave is restricted to the region near the interface, thereby minimizing the contribution from the liquid (*24*). In addition to the degradation processes of the PhACs, the catalytic ozonation mechanism was verified in alumina-supported MnO_x aqueous suspension.

Experimental Section

Materials. Four of the pharmaceuticals—phenazone (PZ), diphenhydramine (DP), phenytoin (PHT), and diclofenac sodium (DS) were purchased from Acros (Geel, Belgium), and ibuprofen (IBU) was obtained from TCI Japan (Tokyo, Japan). Their purities were higher than 99%. Their molecular structures are shown in the Supporting Information (Figure S1). Aluminum isopropoxide [$Al(O_iPr)_3$], glucose, and CA were

* Corresponding author phone: +86-10-62849628; fax: +86-10-62923541; e-mail: huchun@rcees.ac.cn.

10.1021/es803253c CCC: $40.75
Published on Web 03/05/2009

purchased from Beijing Chemical Reagents (Beijing, China). Manganese acetate tetrahydrate was acquired from YiLi (Beijing, China) and commercial mesoporous alumina from Wenzhou Jingjing Alumina (Wenzhou, China). All other reagents were of analytical grade and used as received. All solutions were prepared with deionized water. The pH of the solution was adjusted with HCl or NaOH.

Catalyst Preparation. MA was prepared from precursors of $Al(O_iPr)_3$ in the presence of glucose in an aqueous system, as described previously (*25*). Then MnO_x was supported on MA by the incipient wetness impregnation method with manganese acetate tetrahydrate [$Mn(CH_3COO)_2 \cdot 4H_2O$] as the metal precursor. For example, 0.36 g of manganese acetate tetrahydrate was dissolved in 1.2 cm^3 of distilled water, and 2 g of MA was added to this solution. After impregnation for 2 h, the sample was dried at 383 K for 2 h and finally calcined in a muffle furnace (exposed to static air) at 723 K for 3 h at a heating rate of 0.083 K/s (5 K/min), and then cooled to room temperature naturally. Following this procedure, catalysts were prepared with manganese contents ranging from 0.63 to 6.3 wt %; the catalyst with 3.7 wt % Mn exhibited the highest activity (designated MnO_x/MA) and was used for all subsequent experiments. The weight percent of manganese was calculated by the ratio of the dosed Mn in manganese acetate tetrahydrate to the total dosage of γ-Al_2O_3 and Mn. As a reference, 3.7 wt % Mn was supported on CMA and CA according to the same procedure. These catalysts were designated MnO_x/CMA and MnO_x/CA, respectively.

Characterization. Nitrogen adsorption/desorption experiments of various samples were carried out using a Micromeritics ASAP2000 analyzer (Micromeritics, Norcross, GA). Powder X-ray diffraction (XRD) of the catalyst was recorded on an XDS-2000 diffractometer (Scintag, Cupertino, CA) with Cu Kα radiation ($\lambda = 1.540\ 59$ Å). X-ray photoelectron spectroscopy (XPS) data were taken on an AXIS-Ultra instrument from Kratos (Manchester, UK) using monochromatic Al Kα radiation (225 W, 15 mA, 15 kV) and low-energy electron flooding for charge compensation. Manganese concentrations on the whole particle of various catalysts were measured by inductively coupled plasma optical emission spectrometry (ICP-OES) on an Optima 2000 (PerkinElmer, Inc.) instrument (Supporting Information). The ζ-potential of catalysts in the KNO_3 (10^{-3} M) solution was measured with a Zetasizer 2000 (Malvern, Worcestershire, UK) with three consistent readings. All information for FTIR and in situ ATR-FTIR measurements are shown in the Supporting Information.

Procedures and Analysis. Semibatch experiments were carried out with the 1.2-L reactor shown in Figure S2 (Supporting Information). The reaction temperature was maintained at 20 °C. In a typical experiment, 1 L of aqueous suspensions of PhACs at various concentrations and 1.5 g of catalyst powders were placed in the reactor. The solution was continuously magnetically stirred, and 30 mg of gaseous O_3/L oxygen-zone was bubbled into the reactor through the porous plate of the reactor bottom at a 12 L/h flow rate. The initial pH of reaction suspensions was about 7. The same procedures were carried out for the control experiments of ozone alone and sorption, except no catalyst or no ozone was used. The ozone was generated by a laboratory ozonizer (DHX-SS-IG; Harbin Jiujiu Electrochemistry Technology, Harbin City, China) in the reactor. The residual ozone in the off-gas was adsorbed by a KI solution. At given time intervals, samples were withdrawn and filtered through a filter (pore size 0.45 μm; Millipore, Billerica, MA) for analysis. An aliquot of 0.1 M $Na_2S_2O_3$ was subsequently added to the sample to quench the aqueous ozone remaining in the reaction solution. The gaseous ozone concentration was measured using the iodometric titration method. The concentration of ozone dissolved in the aqueous phase was determined using the indigo method, which was 1.2 mg/L unless otherwise noted. The concentration of each PhAC was measured using high-performance liquid chromatography (1200 series; Agilent, Santa Clara, CA) with an Eclipse XDB-C18 column (5 μm, 4.6 × 150 mm; Agilent). The mobile phase was a solution of 60/40 (v/v) acetonitrile−phosphate buffer solution (20 mM, pH 2.5) and a flow rate of 1 mL/min. The total organic carbon (TOC) content of the solution was analyzed using a Phoenix 8000 TOC analyzer. The errors for TOC determination were less than 1%. Gas chromatography−mass spectrometry (GC−MS) analysis and the preparation of samples are described in Supporting Information. All the experiments were repeated three times, and all of the data are the average of the three determinations.

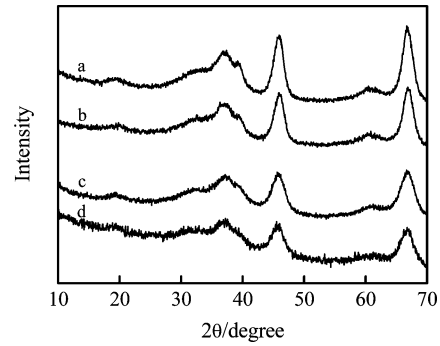

FIGURE 1. XRD patterns of various catalysts: (a) CMA, (b) MnO_x/CMA, (c) MA, and (d) MnO_x/MA.

Results and Discussion

Characterization of Catalysts. These supported manganese oxides, which were prepared by wet impregnation, drying, and calcinations with manganese acetate tetrahydrate as the metal precursor, exist as multivalent oxidation states (*26, 27*). Here, the dispersion of MnO_x on the surfaces of various supports was investigated. Figure S3 (Supporting Information) shows that the nitrogen adsorption/desorption isotherms of MA, MnO_x/MA, and CMA were of type IV with hysteresis loops, which means that the materials had a mesoporous structure, whereas those of CA were generally nonporous. Moreover, both MnO_x/MA and MA had almost identical isotherms, and the pore size distribution of the MnO_x/MA catalyst was nearly identical to that of MA (Supporting Information, Figure S4). Their Brunauer−Emmett−Teller (BET) surface areas were about 287 m^2/g. These results indicate that MnO_x has high dispersion on MA. The BET surface areas of CMA and CA were 184 and 35 m^2/g, respectively. The XRD patterns of the various samples are shown in Figure 1. Standard peaks of pure γ-Al_2O_3 can be seen in the diffractograms of MA, MnO_x/MA, CMA, and MnO_x/CMA, whereas CA has a α-Al_2O_3 structure (Supporting Information, Figure S5). No XRD diffraction peaks of MnO_x were observed in these samples. The dispersion of MnO_x on the various samples was further studied in light of the distribution of manganese. Manganese concentrations on the whole particle and on the surface of the particle were measured by analyzing inductively coupled plasma and XPS. Table S1 (Supporting Information) summarizes the analysis results for the various samples. The manganese concentration on the surface phase (1.2 wt % for MnO_x/MA and 1.7 wt % for MnO_x/CMA) was much lower than that in the bulk (3.2 and 2.9 wt %, respectively). This indicates that most manganese oxide is dispersed into the pore channels, resulting in little being dispersed on the surfaces of MA and CMA. This phenomenon did not occur for MnO_x/CA: the surface manganese concentration (4.6 wt %) was much higher than that in the bulk (2.7 wt %).

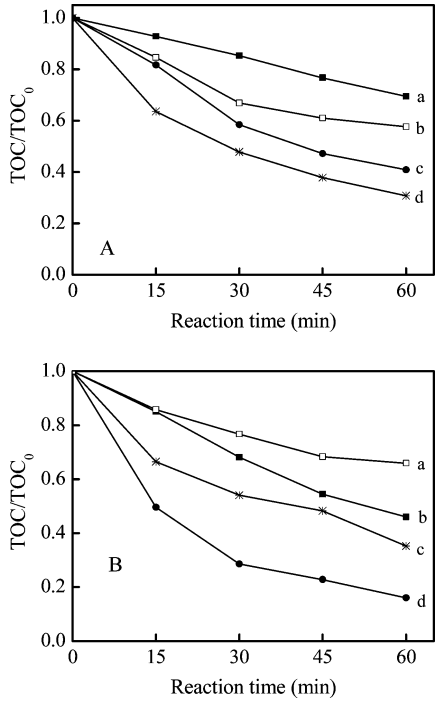

FIGURE 2. TOC removal during the degradation of PZ (40 mg/L) in aqueous dispersions of various catalysts with ozone. (A) With various supports: (a) without catalyst, (b) CA, (c) CMA, and (d) MA. (B) With variously supported MnO_x: (a) Mn^{2+}, (b) MnO_x/CA, (c) MnO_x/CMA, and (d) MnO_x/MA (pH 7.0, catalyst concentration = 1.5 g/L, gaseous ozone concentration = 30 mg/L).

Catalytic Ozonation of Selected PhACs. *Performance of Various Catalysts.* The catalytic activity of various catalysts was evaluated by the degradation of PZ (40 mg/L) with ozone at an initial pH 7. As shown in Figure 2A, only 30% of the TOC was removed at a reaction time of 60 min in the presence of ozone alone. The three supports showed different catalytic activity that gradually decreased in the following order: MA > CMA > CA. Correspondingly, with the introduction of MnO_x, the removal efficiency of PZ increased. About 84%, 65%, and 54% of the TOC, respectively, were removed at a reaction time of 60 min in MnO_x/MA, MnO_x/CMA, and MnO_x/CA suspensions with ozone (Figure 2B). The catalytic activity of MA was most enhanced by the loading of MnO_x. Meanwhile, 34% of the TOC was removed in Mn^{2+} 1.22 mg/L (the highest concentration detected in MnO_x/MA during the reaction at pH 7) solution with ozone, which was almost the same as ozone alone. The catalytic contribution of homogeneous Mn^{2+} was not predominant in this reaction system. The activity of solid catalyst in aqueous solution is related to its surface charge properties. According to ζ-potential measurement, the respective isoelectric points of MA, CMA, and CA were pH 8.6, 8.3, and 7.6. The higher pH of isoelectric points could be responsible for their higher ligand exchange ability (*21*). Therefore, the bigger BET surface area and the surface charge properties of MA result in its higher reactivity. These results show that the nature of the support and the dispersion of manganese on the support markedly affect catalytic activity.

Degradation of Selected PhACs. Figure 3 shows the TOC removal of various PhACs at 3 mg/L in MnO_x/MA suspensions with ozone. Within 40 min, TOC removal of all PhACs except IBU was greater than 90%, whereas TOC removal of IBU was 70%. For DS and PHT in particular, TOC removal reached 90% at a reaction time of 15 min. In contrast, TOC removal efficiency by ozone alone was lower, only about 20% for the PhACs, as shown in the inset to Figure 3. The results show

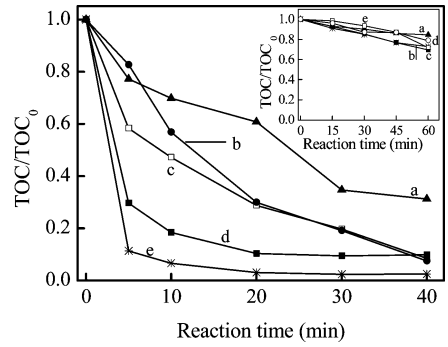

FIGURE 3. TOC removal during the degradation of each PhAC (3 mg/L) in aqueous dispersions of MnO_x/MA with ozone: (a) IBU, (b) DP, (c) PZ, (d) PHT, (e) DS. The inset shows TOC removal of the corresponding PhAC with ozone alone (pH 7.0, catalyst concentration = 1.5 g/L, gaseous ozone concentration = 30 mg/L).

that the MnO_x/MA catalyst is highly effective for the mineralization of various PhACs in the aqueous solution. Furthermore, GC−MS was used to monitor the generation of reaction intermediates during the degradation of the PhACs. All of the identified compounds were unequivocally identified using the NIST98 library database with fit values higher than 90%. Table S2 (Supporting Information) shows the main intermediates from the degradation of PZ, IBU, DP, PHT, and DS at a reaction time of 5 min. Resorcinol, hydroquinone, benzoic or terephthalic acid, hydroxylated aromatic compounds, aliphatic acids, and alcohol were detected in the reaction solution of the PhACs. The aromatic compound disappeared at a reaction time of 30 min, except in the reaction system of IBU, which was oxidized with more difficulty; the main byproducts were aliphatic acids and alcohol. The results demonstrate that the catalytic ozonation of PhACs proceeds by the hydroxylation of substitute groups, followed by the opening of phenyl rings to form small molecular organic acids or diols (or triols) into carbon dioxide and water. In the process with ozone alone, at a reaction time of 5 min, the byproducts from the degradation of PZ, IBU, DP, PHT, and DS were nearly the same as those from the catalyst suspension with ozone (data not shown). However, at a reaction time of 30 min, these byproducts still remained in the solution, suggesting that oxidation performance of ozone is not enough for the further degradation of these intermediates. The effect of pH on TOC removal is shown in the Supporting Information (Figure S6). In the initially tested pH range of 5−9, catalyst activity did not change greatly, while the removal rate is also similar with ozone alone under otherwise identified conditions. In the all experiments, PZ had hardly any adsorption on the surface of the catalyst, indicating that the degradation of PZ occurs predominantly in the solution phase. This result suggested that more free $^{\bullet}OH$ in solution was generated by the catalytic transformation of ozone in MnO_x/MA suspensions.

Catalytic Ozonation Mechanism on Supported MnO_x. On the basis of the mechanism of gas ozone destruction, both Brönsted and Lewis acid sites on the catalyst surface are thought to be the catalytic centers (*28*). The presence of comparatively strong Lewis acid sites on alumina (*18, 29*) leads to the adsorption of Lewis bases such as water and ozone. Therefore, in the present work, surface changes of variously supported MnO_x catalysts were characterized during ozone decomposition using FTIR and in situ ATR-FTIR. The samples for FTIR were prepared by drying catalyst suspensions with or without ozone/PZ overnight in air at 353 K (Supporting Information).

As shown in Figure 4A, the FTIR spectra of the fresh catalysts exhibited only the bands of adsorbed water and hydroxyl groups on the surfaces of these catalysts (1642 and

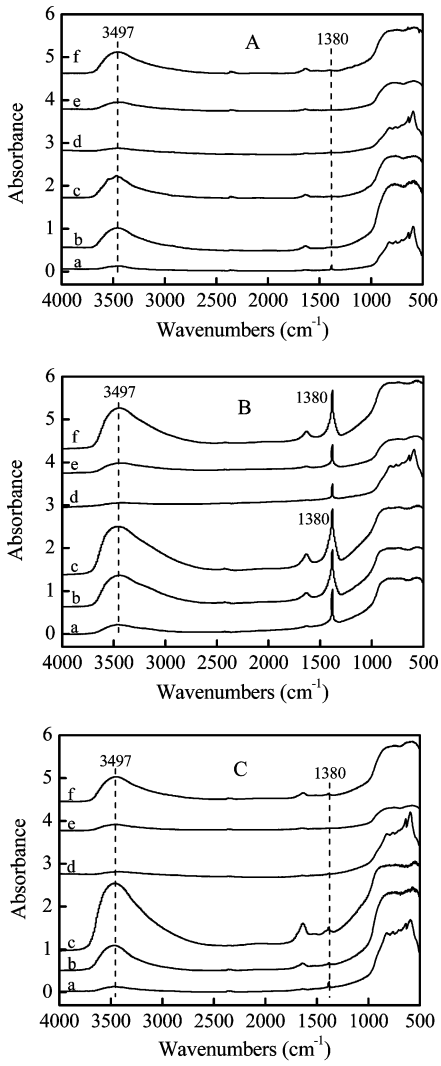

FIGURE 4. FTIR spectra of various processes. (A) Unozonated samples (B) after treatment with ozone solution and (C) after use in aqueous mixture of ozone and PZ. For all panels, (a) CA, (b) CMA, (c) MA, (d) MnO_x/CA, (e) MnO_x/CMA, and (f) MnO_x/MA.

3497 cm^{-1}), except that CA and MnO_x/CA did not have the bands of adsorbed water at 1642 cm^{-1}. After the ozone was added to the catalyst suspensions, a new band appeared around 1380 cm^{-1} in all spectra of the dry catalysts in Figure 4B. Compared with the spectra of different catalysts, the intensities of the peak at 1380 cm^{-1} increased according to the following two orders: CA < CMA < MA and MnO_x/CA < MnO_x/CMA < MnO_x/MA. These orders closely paralleled the catalytic activity of the different catalysts. The same feature peak produced by the treatment of alumina with ozone was observed by Roscoe and Abbatt (*30*). They verified in detail that the peak contributed to a surface oxide species formed by the interaction of ozone with Lewis acid sites on the alumina surface and that the presence of water strongly inhibited the formation of the spectral feature at 1380 cm^{-1} (*30*). However, in the present experiment, the peak at 1380 cm^{-1} appeared after the ozone suspension was dry. A similar surface oxide species was found in the ozonated activated particle by FTIR (*31*). These suggest that the peak quite possibly belongs to the surface oxide species. Meanwhile, with the addition of ozone, the intensities of the hydroxyl groups at 3497 cm^{-1} increased for all samples (comparing Figure 4A and 4B). In particular, a significant increase was observed for MA and MnO_x/MA (Supporting Information, Figure S7). The results reveal that new surface hydroxyl groups

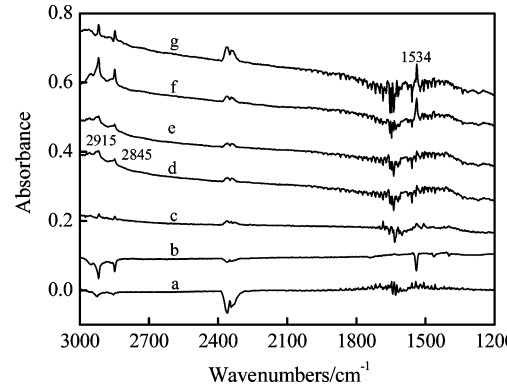

FIGURE 5. ATR-FTIR spectra of different reactions under various conditions in water: (a) ozone alone, (b) MA, (c) MnO_x/MA, (d) MA + O_3, (e) MA + O_3 + PZ, (f) MnO_x/MA + O_3, (g) MnO_x/MA + O_3 + PZ.

form from adsorbed water by hydrogen binding to the surface of the catalyst, which were caused by the interaction of the catalyst with ozone in the aqueous suspension. The phenomenon is in line with that observed by Roscoe and Abbatt (*30*). Similar results were shown by Ma and Graham (*20*). When PZ was added to the suspensions of the catalyst with ozone, the spectra of the dry catalysts did not exhibit the feature peak at 1380 cm^{-1} seen in Figure 4C. Moreover, the intensities of the peak at 3497 cm^{-1} from the surface hydroxyl group decreased for the three supported MnO_x catalysts, whereas those of the three supports did not change. This result indicates that surface oxide species were active sites for the catalytic ozonation of PhACs, whereas surface hydroxyl groups became active sites in the presence of MnO_x.

Furthermore, an in situ ATR-FTIR study of catalytic ozonation in aqueous MnO_x/MA suspensions was carried out (data illustration in Figure S8, Supporting Information). As shown in Figure 5, neither MnO_x/MA and MA suspensions without ozone nor ozone aqueous solutions showed any adsorption peak (curves a−c). When ozone was added to the catalyst suspensions, new bands appeared at 2915 and 2845 cm^{-1}, assigned to surface hydroxyl groups of the catalysts (*30, 32*), and those of MnO_x/MA (curve f) were stronger than those of MA (curve d). Furthermore, the intensities of both peaks decreased with the degradation of PZ for MnO_x/MA (curve g), whereas those of MA did not change (curve e). These results reveal that the introduction of MnO_x enhances the formation and activation of new surface hydroxyl groups in the degradation of PZ. The peak at 1380 cm^{-1} was not observed in in situ ATR-FTIR, due to the role of water. The results verify that surface oxide species can react with H_2O to generate surface sites of hydroxyl groups. The peak position of hydroxyl groups observed in in situ ATR-FTIR was different from that one in FTIR. This is possibly attributable to different experimental conditions. The former spectra were obtained in water, whereas the latter were obtained under dry conditions. The other new peak at 1534 cm^{-1} appeared in the spectra of MA and MnO_x/MA with ozone (Figure 5). Its intensity did not change with the addition of PZ, indicating that it was not an active site for the degradation.

In all of the experiments of catalytic ozonation of PhACs, no significant adsorption was observed for any PhAC at various pH levels. This result verifies that the oxidation reactions of PhACs occur mainly in the aqueous phase, not on the surface of the catalyst. The active species were investigated with regard to the catalytic ozonation of MnO_x/MA. *tert*-Butyl alcohol is a strong radical scavenger that has a reaction rate constant of 6×10^8 M^{-1} s^{-1} with hydroxyl radicals and only 3×10^{-3} M^{-1} s^{-1} with ozone. It can terminate radical chain reactions by generating inert intermediates. Thus, *tert*-butyl alcohol was adopted as the indicator for a

radical-type reaction. At pH 7, IBU was barely adsorbed on the surface of MnO_x/MA. The oxidation reaction of IBU occurred mainly in solution. As shown in Figure S9 (Supporting Information), the degradation of IBU was not depressed with the addition of *tert*-butyl alcohol under ozonation alone. In contrast, in MnO_x/MA suspensions with ozone, it was significantly depressed with the addition of *tert*-butyl alcohol. Moreover, the reaction rate was similar to that for ozone alone. These results indicate that hydroxyl radicals are the main active species in catalytic ozonation. In light of the experimental data and a review of the literature (*28*, *31*), a mechanism is proposed for the catalytic ozonation of PhACs in MnO_x/MA suspension (Supporting Information, Table S3). In this process, a new surface hydroxyl group forms from the interaction of water with Lewis acid sites on MA. Subsequently, the new surface hydroxyl groups act as Brönsted acid sites and adsorb ozone to form surface complex $\equiv SOH(O_3)_s$ (S refers to the surface of the catalyst), and then the ozone is catalytically transformed into $^{\bullet}OH$ and $^{\bullet}O_3-S$ by MnO_x. Interfacial electron transfer is involved in the catalytic decomposition reaction of ozone. The multivalent MnO_x has two redox couples (Mn^{3+}/Mn^{2+} and Mn^{4+}/Mn^{3+}) enhancing the electron transfer, resulting in higher activity.

Acknowledgments

This work was supported by the National Natural Science Foundation of China (No. 50621804 to J.Q.) and the Chinese Academy of Sciences (No. kzcx1-yw-06 to J.L. and RCEES-QN-200704 to X.H).

Supporting Information Available

The structure of selected pharmaceuticals, N_2 adsorption/desorption isotherms and pore size distribution of various samples, XRD patterns of CA and MnO_x/CA, FTIR and ATR-FTIR spectra, effects of pH and *tert*-butyl alcohol on the reaction, bulk and surface manganese concentrations, GC−MS analysis, and in situ ATR-FTIR and FTIR experiments. This material is available free of charge via the Internet at http://pubs.acs.org.

Literature Cited

(1) Heberer, T. Occurrence, fate, and removal of pharmaceutical residues in the aquatic environment: A review of recent research data. *Toxicol. Lett.* **2002**, *131* (1−2), 5–17.
(2) Kolpin, D. W.; Furlong, E. T.; Meyer, M. T.; Thurman, E. M.; Zaugg, S. D.; Barber, L. B.; Buxton, H. T. Pharmaceuticals, hormones, and other organic wastewater contaminants in U.S. streams, 1999−2000: A national reconnaissance. *Environ. Sci. Technol.* **2002**, *36* (6), 1202–1211.
(3) Fent, K.; Weston, A. A.; Caminada, D. Ecotoxicology of human pharmaceuticals. *Aquat. Toxicol* **2006**, *76* (2), 122–159.
(4) Jones, O. A.; Lester, J. N.; Voulvoulis, N. Pharmaceuticals: A threat to drinking water. *Trends Biotechnol* **2005**, *23* (4), 163–167.
(5) Ternes, T. A. Pharmaceuticals and metabolites as contaminants of the aquatic environment. In *Pharmaceuticals and Personal Care Products in the Environment: Scientific and Regulatory Issues*; Daughton, C. G., Jones-Lepp, T. L., Eds.; ACS Symposium Series 791; American Chemical Society: Washington, DC, 2001; pp 39−54.
(6) Loraine, G. A.; Pettigrove, M. E. Seasonal variations in concentrations of pharmaceuticals and personal care products in drinking water and reclaimed wastewater in Southern California. *Environ. Sci. Technol.* **2006**, *40* (3), 687–695.
(7) Pomati, F.; Netting, A. G.; Calamari, D.; Neilan, B. A. Effects of erythromycin, tetracycline and ibuprofen on the growth of *Synechocystis* sp. and *Lemna minor*. *Aquat. Toxicol* **2004**, *67* (4), 387–396.
(8) Pomati, F.; Castiglioni, S.; Zuccato, E.; Fanelli, R.; Vigetti, D.; Rossetti, C.; Calamari, D. Effects of a complex mixture of therapeutic drugs at environmental levels on human embryonic cells. *Environ. Sci. Technol.* **2006**, *40* (7), 2442–2447.
(9) Andreozzi, R.; Insola, A.; Caprio, V.; Marotta, R.; Tufano, V. The use of manganese dioxide as a heterogeneous catalyst for oxalic acid ozonation in aqueous solution. *Appl. Catal., A* **1996**, *138* (1), 75–81.
(10) Legube, B.; Karpel Vel Leitner, N. Catalytic ozonation: A promising advanced oxidation technology for water treatment. *Catal. Today* **1999**, *53* (1), 61–72.
(11) Kasprzyk-Hordern, B.; Raczyk-Stanislawiak, U.; Swietlik, J.; Nawrocki, J. Catalytic ozonation of natural organic matter on alumina. *Appl. Catal., B* **2006**, *62* (3−4), 345–358.
(12) Beltrán, F. J.; Rivas, F. J.; Montero-de-Espinosa, R. A TiO_2/Al_2O_3 catalyst to improve the ozonation of oxalic acid in water. *Appl. Catal., B* **2004**, *47* (2), 101–109.
(13) Konova, P.; Stoyanova, M.; Naydenov, A.; Christoskova, S.; Mehandjiev, D. Catalytic oxidation of VOCs and CO by ozone over alumina supported cobalt oxide. *Appl. Catal., A* **2006**, *298*, 109–114.
(14) Einaga, H.; Ogata, A. Benzene oxidation with ozone over supported manganese oxide catalysts: Effect of catalyst support and reaction conditions. *J. Hazard. Mater.* **2009**, in press (DOI: 10.1016/j.jhazmat.2008.09.032).
(15) Einaga, H.; Futamura, S. Comparative study on the catalytic activities of alumina-supported metal oxides for oxidation of benzene and cyclohexane with ozone. *React. Kinet. Catal. Lett.* **2004**, *81*, 121–128.
(16) Li, W.; Gibbs, G.; Oyama, S. Mechanism of ozone decomposition on a manganese oxide catalyst. 1. In situ Raman spectroscopy and ab initio molecular orbital calculations. *J. Am. Chem. Soc.* **1998**, *120* (35), 9041–9046.
(17) Radhakrishnan, R.; Oyama, S. T.; Ohminami, Y.; Asakura, K. Structure of MnO_x/Al_2O_3 catalyst: A study using EXAFS, in situ laser Raman spectroscopy and ab initio calculations. *J. Phys. Chem. B* **2001**, *105* (38), 9067–9070.
(18) Bulanin, K. M.; Lavalley, J. C.; Tsyganenko, A. A. IR spectra of adsorbed ozone. *Colloids Surf., A* **1995**, *101* (2−3), 153–158.
(19) Beltrán, F. J.; Rivas, F. J.; Montero-de-Espinosa, R. Catalytic ozonation of oxalic acid in an aqueous TiO_2 slurry reactor. *Appl. Catal., B* **2002**, *39* (3), 221–231.
(20) Ma, J.; Graham, N. J. D. Degradation of atrazine by manganese-catalysed ozonation: Influence of humic substances. *Water Res.* **1999**, *33* (3), 785–793.
(21) Zhang, T.; Li, C.; Ma, J.; Tian, H.; Qiang, Z. Surface hydroxyl groups of synthetic α-FeOOH in promoting $^{\bullet}OH$ generation from aqueous ozone: Property and activity relationship. *Appl. Catal., B* **2008**, *82* (1−2), 131–137.
(22) Joseph, Y.; Ranke, W.; Weiss, W. Water on FeO(111) and Fe_3O_4(111): Adsorption behavior on different surface terminations. *J. Phys. Chem. B* **2000**, *104* (14), 3224–3236.
(23) Heberer, T. Tracking persistent pharmaceutical residues from municipal sewage to drinking water. *J. Hydrol.* **2002**, *266* (3−4), 175–189.
(24) Harrick, N. J. *Internal Reflection Spectrocopy*; Interscience: New York, 1967.
(25) Xu, B.; Xiao, T.; Yan, Z.; Sun, X.; Sloan, J.; González-Cortés, S. L.; Alshahrani, F.; Green, M. L. H. Synthesis of mesoporous alumina with highly thermal stability using glucose template in aqueous system. *Microporous Mesoporous Mater.* **2006**, *91* (1−3), 293–295.
(26) Kijlstra, W. S.; Poels, E. K.; Bliek, A.; Weckhuysen, B. M.; Schoonheydt, R. A. Characterization of Al_2O_3-supported manganese oxides by electron spin resonance and diffuse reflectance spectroscopy. *J. Phys. Chem. B* **1997**, *101* (3), 309–316.
(27) Xing, S.; Hu, C.; Qu, J.; He, H.; Yang, M. Characterization and reactivity of MnO_x supported on mesoporous zirconia for herbicide 2,4-D mineralization with ozone. *Environ. Sci. Technol.* **2008**, *42* (9), 3363–3368.
(28) Kasprzyk-Hordern, B.; Zióek, M.; Nawrocki, J. Catalytic ozonation and methods of enhancing molecular ozone reactions in water treatment. *Appl. Catal., B* **2003**, *46* (4), 639–669.
(29) Al-Abadleh, H. A.; Grassian, V. H. FT-IR study of water adsorption on aluminum oxide surfaces. *Langmuir* **2003**, *19* (2), 341–347.
(30) Roscoe, J. M.; Abbatt, J. P. D. Diffuse reflectance FTIR study of the interaction of alumina surfaces with ozone and water vapor. *J. Phys. Chem. A* **2005**, *109* (40), 9028–9034.
(31) Beltrán, F. J.; Rivas, J.; Álvarez, P.; Montero-de-Espinosa, R. Kinetics of heterogeneous catalytic ozone decomposition in water on an activated carbon. *Ozone Sci. Eng.* **2002**, *24*, 227–237.
(32) Tejedor-Tejedor, M. I.; Anderson, M. A. "In situ" attenuated total reflection fourier transform infrared studies of the goethite (α-FeOOH)−aqueous solution interface. *Langmuir* **1986**, *2*, 203–210.

ES803253C